

pubs.acs.org/estengg Article

Using Building Energy and Smart Thermostat Data to Evaluate Indoor Ultrafine Particle Source and Loss Processes in a Net-Zero Energy House

Jinglin Jiang, Nusrat Jung, and Brandon E. Boor*



Cite This: https://doi.org/10.1021/acsestengg.1c00002



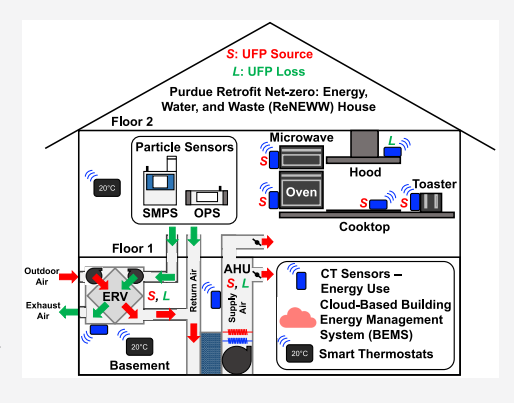
ACCESS

Metrics & More

Article Recommendations

Supporting Information

ABSTRACT: The integration of Internet of Things (IoT)-enabled sensors and building energy management systems (BEMS) into smart buildings offers a platform for real-time monitoring of myriad factors that shape indoor air quality. This study explores the application of building energy and smart thermostat data to evaluate indoor ultrafine particle dynamics (UFP, diameter ≤ 100 nm). A new framework is developed whereby a cloud-based BEMS and smart thermostats are integrated with real time UFP sensing and a material balance model to characterize UFP source and loss processes. The data-driven framework was evaluated through a field campaign conducted in an occupied net-zero energy building—the Purdue Retrofit Net-zero: Energy, Water, and Waste (ReNEWW) House. Indoor UFP source events were identified through time-resolved electrical kitchen appliance energy use profiles derived from BEMS data. This enabled determination of kitchen appliance-resolved UFP source rates and time-averaged concentrations and



size distributions. BEMS and smart thermostat data were used to identify the operational mode and runtime profiles of the air handling unit and energy recovery ventilator, from which UFP source and loss rates were estimated for each mode. The framework demonstrates that equipment-level energy use data can be used to understand how occupant activities and building systems affect indoor air quality.

KEYWORDS: data-driven indoor air quality, particulate matter, smart buildings, IoT sensors, building systems

■ INTRODUCTION

Residential buildings are complex engineering systems. Their design and operation plays a significant role in modulating our exposure to air pollutants of indoor and outdoor origin since we spend approximately 90% of our time indoors.^{1–4} Heating, ventilation, and air conditioning (HVAC) systems are of particular importance, as they often serve as the interface between indoor and outdoor atmospheres and incorporate various filtration technologies for pollutant removal.^{5–8} Another intrinsic element of residential building systems are occupants, who interact intimately with their surrounding indoor environments. Occupant activities, such as cooking and cleaning, drive profound changes in the composition of indoor air.^{3,9–16} Thus, both HVAC systems and occupant activities need to be jointly considered when evaluating indoor air pollutant source and loss processes.

A holistic characterization of residential building systems is necessary to understand the factors that affect indoor air pollutant concentrations. Smart buildings that incorporate Internet of Things (IoT)-enabled sensors and devices that are integrated with cloud-based building energy management systems (BEMS) can monitor HVAC systems and occupancy in real time, ^{17–27} providing a foundation for data-driven indoor air quality assessment and ventilation control. Smart building

technology is becoming essential in the transition toward netzero energy buildings (NZEBs), ²⁸⁻³⁴ which integrate intelligent management of energy-efficient HVAC systems, electrical appliances, and lighting with on-site energy production. ^{30,35} However, indoor air quality field investigations in smart buildings, NZEBs, and similarly designed high-performance/passive homes are limited. ^{13,33,36-41}

Smart buildings and NZEBs are commonly retrofitted with smart meters, current transducer (CT) sensors, smart thermostats, and BEMS for real time monitoring of building- and appliance-level energy consumption and use profiles. ^{18,22,35,42–44} Such sensing and data management systems offer exciting possibilities for evaluating how HVAC systems and electrical appliances impact indoor air quality. Several studies have used CT sensors and smart thermostats for evaluating HVAC system runtime (fractional on-time). ^{20,43,45,46} However,

Received: January 5, 2021
Revised: February 24, 2021
Accepted: March 3, 2021



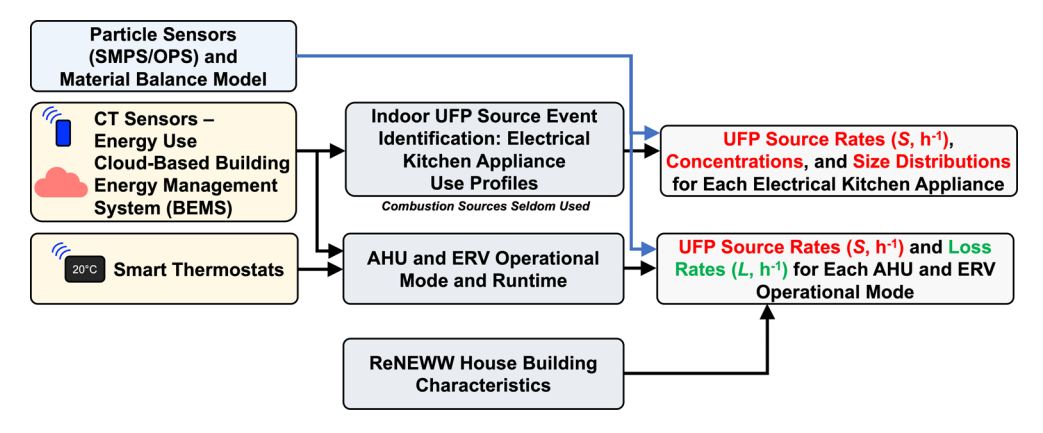


Figure 1. Flow diagram illustrating how the ReNEWW House sensing platform is used for indoor UFP source event identification, evaluation of AHU and ERV operational mode and runtime, and UFP source and loss processes attributed to electrical kitchen appliances and operation of the AHU and ERV.

a comprehensive framework for using building energy and smart device data to characterize indoor air pollutant dynamics in smart homes is lacking.

The objective of this study is to develop and evaluate a data-driven framework for characterizing indoor air pollutant source and loss processes in a residential NZEB through the use of CT sensors, a cloud-based BEMS, and smart thermostats. This study takes a systems-level approach and considers both HVAC- and occupant-associated processes that affect indoor air quality. The framework is centered on evaluating indoor ultrafine particles (UFPs, diameter \leq 100 nm), which can penetrate deep into the respiratory system and are associated with numerous adverse toxicological and human health outcomes. The study considers UFP source and loss processes associated with occupant-initiated cooking with electrical kitchen appliances and the operation of an energy-efficient HVAC system with an energy recovery ventilator (ERV) for outdoor air intake.

MATERIALS AND METHODS

Site Description: Residential Net-Zero Energy Building—Purdue ReNEWW House. The data-driven framework for characterizing indoor UFP source and loss processes (Figure 1) was developed and evaluated through a one-month field measurement campaign conducted in an occupied residential NZEB—the Purdue Retrofit Net-zero: Energy, Water, and Waste (ReNEWW) House (Figure S1). The ReNEWW House is located at Purdue University in West Lafayette, IN, U.S.A. The three-story detached home (266 m² total conditioned area) was built in 1928 and underwent a deep energy retrofit between 2014 and 2015, as described in detail elsewhere. 23,35,42,61 The house was occupied by three adult residents during the campaign. The ReNEWW House is partitioned into a belowground basement, which houses an air handling unit (AHU, Figure S2) and ERV (Figure S3); floor 1, which includes an open-concept kitchen equipped with all electrical appliances (Figure S4), including an electric induction cooktop, oven, toaster, microwave, and ductless range hood; and floor 2, which includes three bedrooms. The directionality of airflows associated with the AHU/ERV is as follows: the AHU delivers damper-modulated supply air to the basement and floor 1; return air is directed from floor 1 to the ERV (for exhaust to the outdoors) and the AHU (for recirculation); and the ERV delivers outdoor air to the AHU, where it mixes with return air prior to in-duct filtration (via MERV 11 filter) and heating/

cooling. The AHU includes one blower, and the ERV includes two blowers, one each for intake and exhaust.

ReNEWW House Sensing Platform for Collecting Building Energy, Smart Thermostat, and UFP Data. The Purdue ReNEWW House is equipped with a comprehensive data monitoring system that incorporates an extensive array of sensors and data acquisition (DAQ) units to monitor and record energy consumption/production and indoor environmental conditions throughout the home.³⁵ Equipment-level energy consumption is measured with 150-, 50-, and 20-A CT sensors at a 1 min time resolution. The CT sensors and DAQs are integrated with a cloud-based BEMS (SiteSage, Powerhouse Dynamics Inc.). In this study, only energy consumption data for the AHU, ERV, and electrical kitchen appliances were used. WiFi-enabled smart thermostats (ecobee3 Lite, ecobee Inc.) installed in the basement and on floor 1 are used to control the AHU/ERV and monitor floor-level heating/cooling requirements via the set point and measured air temperature. Data is managed via a web portal (ecobee HomeIQ, ecobee Inc.).

Indoor particle number size distributions (cm⁻³) were measured continuously (24 h per day) with a scanning mobility particle sizer (SMPS, electrical mobility diameter (D_{em}) range: 10 to 300 nm) (Model 3910, TSI Inc.) and an optical particle sizer (OPS, optical diameter (Do) range: 300 to 10 000 nm) (Model 3330, TSI Inc.) at 1 min time resolution. Particle number size distributions from $D_{\rm em}$ = 150 to 300 nm were estimated through spline interpolation due to operational limitations of the SMPS. $^{62-65}$ The SMPS and OPS were located on floor 1 between the kitchen and the living room, with sample inlets 1.5 m above the floor. Measured particle number size distributions were translated to surface area (μ m² cm⁻³) and volume (μ m³ cm⁻³) size distributions assuming spherical particles (dynamic shape factor: $\chi = 1$) and mass size distributions ($\mu g \text{ m}^{-3}$) using measured size-resolved effective densities (ρ_{eff}) for indoor particles in the ReNEWW House (Figure S5), following the work of Wu and Boor (2020).66 Particle size distributions were then fit to multimodal log-normal distribution functions.^{67,68} Following completion of the one month measurement campaign, outdoor particle number size distributions were measured for 1 week with the SMPS, OPS, and a silica gel diffusion dryer (Model 3062, TSI Inc.).

Framework for Integrating Building Energy and Smart Thermostat Data with UFP Dynamics. As illustrated in Figure 1, the data-driven framework utilizes the ReNEWW House sensing platform to integrate CT sensors, a cloud-based

BEMS, smart thermostats, and particle sensors (SMPS and OPS; UFPs via SMPS only) to evaluate UFP source and loss processes. First, the CT sensors and BEMS are used to identify indoor UFP source events associated with the use of the electrical kitchen appliances for cooking—electric induction cooktop, oven, toaster, and microwave. Time-resolved use profiles were determined for each kitchen appliance via the BEMS data, enabling determination of the number and duration of cooking-associated indoor UFP source events (Table 1).

Table 1. Indoor UFP Source Event Identification at the Purdue ReNEWW House: Number and Duration of Indoor UFP Source Events Associated with Electrical Kitchen Appliances as Determined by BEMS Data^a

			source event duration [min]		
indoor UFP source events identified with BEMS data	total no. identified with BEMS data	no. of events available for source rate estimation	median	minimum	maximum
cooktop	24	17	10.5	3	26
oven	13 ^b	10	29	16	49
toaster	48	21	5	4	9
microwave	55 ^c	32	4.5	3	17
UFP events not associated with electrical kitch- en appliances	7	-	-	-	-

"Both the total number of events and those available for UFP source rate estimation are listed. UFP events not associated with electrical kitchen appliances were identified with UFP data when UFP concentrations increased, but no kitchen appliances were active. Source events are used to determine UFP source rates (S) and time-averaged concentrations and size distributions for each electrical kitchen appliance (S not estimated for the microwave due to low UFP concentrations). Doven events that occurred within 1 h were considered as a single event. Microwave events that occurred within 10 min were considered as a single event.

Second, the CT sensors, BEMS, and smart thermostats were used to identify the operational mode and runtime^{20,43,45,46} of the AHU and ERV (Table 2); the AHU and ERV can act as both

Table 2. AHU and ERV Operational Modes at the Purdue ReNEWW House as Determined by BEMS and Smart Thermostat Data and the Number of Occurrences for Each Mode from Which Total UFP Loss Rates (L) Were Estimated during UFP Concentration Decays

Purdue ReNEWW House AHU and ERV operational mode	no. for estimating UFP loss rates (L)
Mode 1: AHU Off, ERV Off	17
Mode 2: AHU On, ERV Off, Floor 1 Heating On	14
Mode 3: AHU On, ERV On, Floor 1 Heating Off	29
Mode 4: AHU On, ERV On, Floor 1 Heating On	4

a source and loss for UFPs. Third, time-averaged UFP concentrations and size distributions for each kitchen appliance were characterized. This is done by incorporating the BEMS-derived kitchen appliance use profiles with UFP data. Fourth, a material balance model (eq 1) was developed to estimate UFP source rates (S, h^{-1}) for each kitchen appliance and each AHU/ERV operational mode and loss rates (L, h^{-1}) for each AHU/

ERV operational mode (Table 2), using the associated UFP

AHU and ERV Operational Modes. Over the duration of the measurement campaign, four operational modes for the AHU and ERV were identified via the BEMS and smart thermostat data: (1) AHU off, ERV off; (2) AHU on, ERV off, floor 1 heating on; (3) AHU on, ERV on, floor 1 heating off; and (4) AHU on, ERV on, floor 1 heating on (Table 2). During the campaign, the AHU was found to only operate under the heating mode (mean outdoor temperature of 44 °F (6.67 °C)), and the ERV was found to operate on a preset cycle. It was observed that the AHU can be turned on when either the basement or floor 1 calls for heating as determined by the two smart thermostats (when measured temperature = set point temperature—0.5 °F (0.28 °C)) or when the ERV operates according to its preset cycle, which is independent of the floor-level heating requirements. When the AHU and ERV are both off, there is no call for heating within the house by either smart thermostat. When the AHU is on and the ERV is off, there must be a call for heating in the basement or floor 1. When the AHU and ERV are both on, the heating status was determined by the smart thermostat data to differentiate between modes 3 and 4. Volumetric airflow rates for the supply air (AHU to basement and AHU to floor 1) and return air (floor 1 to AHU and floor 1 to ERV as exhaust) varied among the four operational modes; they were measured with a flow capture hood (Model 6200, TSI Inc.) across all supply and return grilles and summarized in Table S1.

Estimating UFP Source and Loss Rates. A material balance model was used to determine UFP source rates (S, h^{-1}) for the electrical kitchen appliances, AHU, and ERV and total UFP loss rates (L, h^{-1}) for the AHU and ERV. For simplicity, the model treats floor 1 as a single-zone completely mixed flow reactor (CMFR) with a volume of $V = 256 \text{ m}^3$. The SMPS was positioned at a central location on floor 1 between the kitchen and living room so as to prevent sampling in the cooking emission plumes, ⁶⁹ thereby better representing a well-mixed concentration. The model uses size-integrated UFP number concentrations $(N, D_{\rm em} = 10 \text{ to } 100 \text{ nm})$ to derive size-integrated estimates of UFP S and L (for $D_{\rm em} = 10 \text{ to } 100 \text{ nm}$):

$$V\frac{\mathrm{d}N}{\mathrm{d}t} = S - LNV \tag{1}$$

Electrical kitchen appliance-resolved UFP source rates were computed by rearranging eq $1~{\rm as}^{70-73}$

$$S_{KIT} = V \left[\frac{N(t_1) - N(t_0)}{t_1 - t_0} + L\bar{N} \right]$$
 (2)

where $S_{\rm KIT}$ is the time-averaged UFP source rate during an active period of cooking with an electrical kitchen appliance as determined by the BEMS data, $N(t_0)$ and $N(t_1)$ are the initial and maximum UFP number concentrations (cm⁻³) during the cooking period, t_0 and t_1 are the associated times (h) for each, \overline{N} is the average UFP number concentration (cm⁻³) from t_0 to t_1 , and L is the UFP loss rate for the corresponding AHU/ERV operational mode as determined by the BEMS and smart thermostat data. $S_{\rm KIT}$ incorporates the additive effects of UFP emissions due to the cooking process itself (e.g., frying, baking)^{69,74–80} and heated surfaces (e.g., cooktop burner, toaster coils). 81,82 Coagulation is assumed to be negligible as $N < 2 \times 10^4$ cm⁻³ during the cooking events. 83,84 Table 1 lists the number of events for which $S_{\rm KIT}$ was estimated for each appliance.

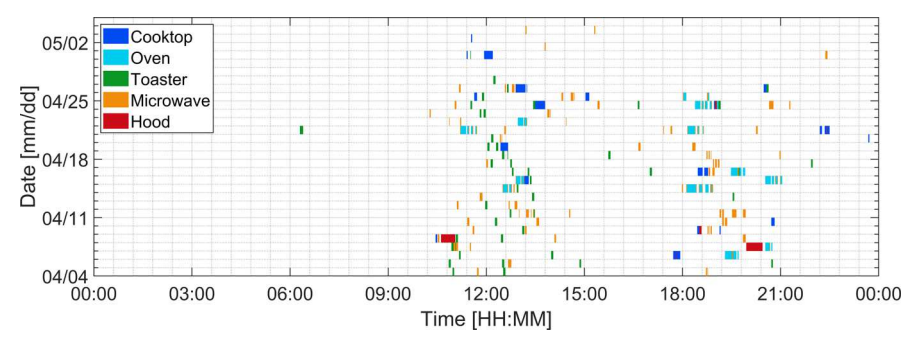


Figure 2. Indoor UFP source event identification at the Purdue ReNEWW House: time-resolved kitchen appliance use profiles derived from BEMS data. Source events are used to determine UFP source rates (*S*) and time-averaged concentrations and size distributions for each electrical kitchen appliance (excluding the hood).

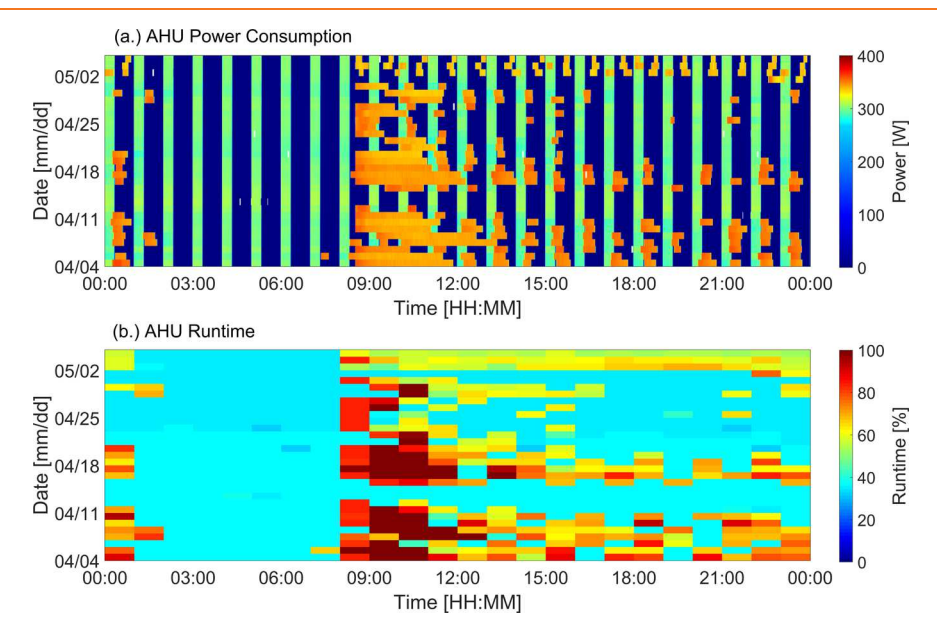


Figure 3. Purdue ReNEWW House AHU (a) time-resolved power consumption profile and (b) time-resolved runtime profile as determined by BEMS data. The colorbar indicates the AHU power consumption in W (for (a)) and runtime percentage (for (b)). The AHU energy use data is used to determine UFP source (S) and loss (L) rates for each AHU/ERV operational mode (Table 2).

UFP loss rates for each of the four AHU/ERV operational modes (Table 2) were obtained through least-squares regression of the UFP number concentration decays 7,85 following a BEMS-identified cooking period. Table 2 lists the number of occurrences for each mode from which UFP loss rates were estimated during the concentration decays. L represents the total rate of removal of UFPs and incorporates the additive effects of (i) deposition to indoor surfaces, $^{86-88}$ (ii) deposition to AHU components (e.g., MERV 11 filter, heating/cooling coils, ducts), 8,89,90 (iii) exhaust to the outdoors via the ERV, (iv) exfiltration through the building envelope, $^{91-93}$ and (v) interzonal air exchange. 94 Thus, the apportionment of L among processes (i)—(v) was not determined. The contribution of the ductless range hood was not considered as it was only used on several occasions (Figure 2).

Time-averaged UFP source rates for the AHU/ERV $(S_{\text{AHU/ERV}})$ were computed during pseudo steady-state periods $(N \sim \text{constant})$ when the electrical kitchen appliances were off by rearranging eq 1 as

$$S_{\text{AHU/ERV}} = L\overline{N}V \tag{3}$$

where \overline{N} is the average UFP number concentration (cm⁻³) during a pseudo-steady-state period for a given AHU/ERV

operational mode as determined by the BEMS and smart thermostat data and L is the UFP loss rate for that mode. UFP source rates for modes 1 and 2 (AHU on/off, ERV off) and modes 3 and 4 (AHU on, ERV on) were aggregated together. $S_{\rm AHU/ERV}$ represents the total rate of UFP introduction to floor 1 of the ReNEWW House and includes the additive effects of (i) intake of outdoor UFPs to the AHU via the ERV, (ii) infiltration through the building envelope, $^{91-93}$ and (iii) interzonal air exchange with the basement. 94 $S_{\rm KIT}$ accounted for all UFP sources during a cooking event, including emissions from cooking itself and sources from the operation of the AHU/ERV. As $S_{\rm AHU/ERV} \ll S_{\rm KIT}$ (Figure 9), $S_{\rm KIT}$ can be considered to be the approximate emission rate for the cooking events.

■ RESULTS AND DISCUSSION

The following sections present elements of the data-driven framework for linking building energy, smart thermostat, and particle data for characterizing indoor UFP source and loss processes in a residential NZEB (Figure 1). First, BEMS-derived electrical kitchen appliance use profiles are presented, which are used for indoor UFP source event identification. Second, AHU/ERV power consumption and runtime profiles are introduced. Third, electrical kitchen appliance-resolved UFP concentrations

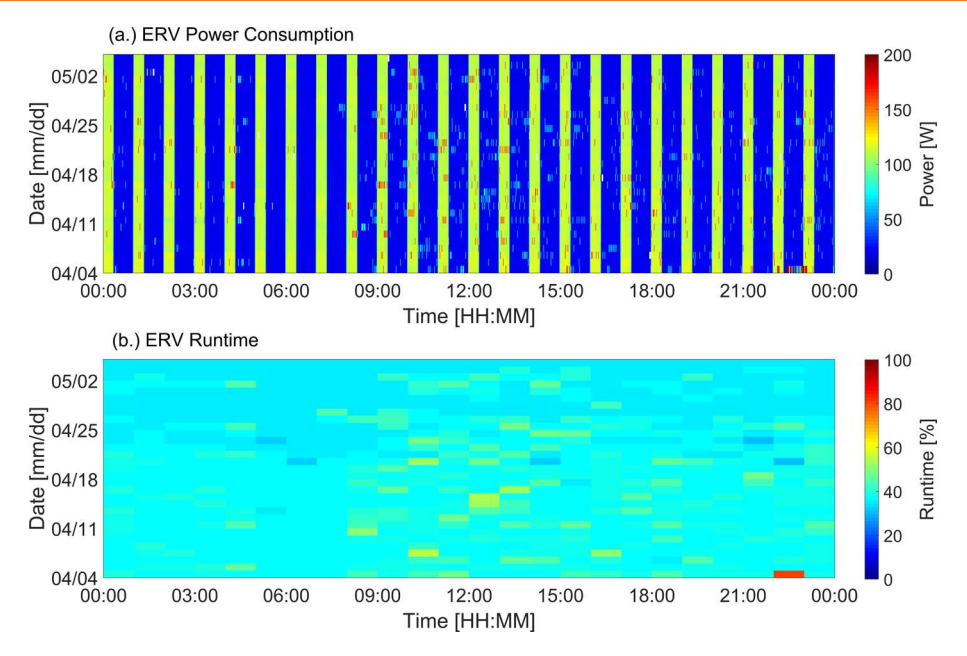


Figure 4. Purdue ReNEWW House ERV (a) time-resolved power consumption profile and (b) time-resolved runtime profile as determined by BEMS data. The colorbar indicates the ERV power consumption in W (for (a)) and runtime percentage (for (b)). The ERV energy use data is used to determine UFP source (S) and loss (L) rates for each AHU/ERV operational mode (Table 2).

and size distributions are discussed. Fourth, UFP source and loss rates estimated for each electrical kitchen appliance and AHU/ERV operational mode are presented.

Electrical Kitchen Appliance Use Profiles Derived from BEMS Data. The data-driven framework uses CT sensors and a cloud-based BEMS to determine when and for how long each electrical kitchen appliance is being used by the occupants of the ReNEWW House. Table 1 summarizes the number and duration of indoor UFP source events associated with the cooktop, oven, toaster, and microwave. It was found that cooking was the primary indoor UFP source as it accounted for 140 of 147 observed UFP source events in the ReNEWW House during the one month campaign. The unassigned 7 UFP source events where measured UFP number concentrations suddenly increased may be associated with the undocumented use of indoor combustion sources (e.g., candles),83 ozonolysisinitiated secondary organic aerosol formation due to use of scented cleaning products and air fresheners, 11,83,95-99 and portable humidifiers, 100–102 among others.

The microwave (n = 55 events) and toaster (n = 48 events)were the most frequently used appliances; however, their median event durations, 4.5 and 5 min, respectively, were comparatively low relative to the cooktop (10.5 min, n = 24events) and oven (29 min, n = 13 events). This is important as the net number of UFPs emitted ($\int S_{KIT} dt$) depends on the duration of the source event. Figure 2 illustrates the BEMSderived temporal use profiles of the kitchen appliances. The majority of the cooking events occurred from 11:00 to 14:00 and 18:00 to 21:00, likely corresponding to meal preparation for lunch and dinner, respectively. Only one cooking event (toaster) was identified via the BEMS data from 00:00 to 10:00, and few events were found to occur between 21:00 and 00:00. The use profiles for the cooktop, oven, toaster, and microwave were fairly consistent during the campaign; however, the ductless range hood was used infrequently. The use of BEMS data to identify when occupant-initiated cooking events are occurring is of value as cooking is an important indoor particle source, 10,11,69,74,75,7

and this approach precludes the use of detailed occupant activity surveys. $^{103,104}\,$

AHU/ERV Power Consumption and Runtime Profiles Derived from BEMS Data. The CT sensors and cloud-based BEMS enabled determination of diurnal power consumption and runtime profiles for the AHU (Figure 3) and ERV (Figure 4). The colorbars in Figures 3a and 4a indicate the power draw (W) of the AHU and ERV, respectively, and provide a useful visualization tool for identifying the temporality of the AHU/ ERV operational mode (Table 2). In Figure 3a, blue (0 W) indicates when the AHU and ERV are both off (mode 1), greenred (250-400 W) indicates when the AHU is on (modes 2-4), green (250-300 W) indicates when the AHU and ERV are on with floor 1 heating off (mode 3), and orange-red (325–400 W) indicates when the AHU is on with floor 1 heating on (modes 2 and 4). Mode 2 can be differentiated from mode 4 by identifying periods when the ERV is off (blue in Figure 4a) but the AHU remains on (red-orange in Figure 3a).

The ERV operates following a preset cycle that repeats continually throughout the day, aside from a few fluctuations in the CT sensor output. The operation of the AHU is more variable. Between 01:00 and 07:00, the smart thermostat data did not show a call for heating and the AHU/ERV operational mode oscillated between modes 1 and 3. Heating on floor 1 is often called for between 08:30 and 12:00, with modes 2 and 4 common. The is due in part to the temperature set point of the floor 1 smart thermostat, which increased from 66 °F (18.9 °C) to 70 °F (21.1 °C) at 08:30 (it remained at 70 °F (21.1 °C) until 01:00, when it changed back to 66 °F). From 12:00 to 00:00, heating is called for less frequently and the AHU/ERV oscillate between all four modes. Modes 2 and 4 became less common during the later stages of the campaign as the outdoor air temperature increased and the demand for heating was reduced.

The diurnal hourly runtime (eq 4, the percentage of time the AHU/ERV were active in 1 h: 0 to 100%) profiles for the AHU (Figure 3b) and ERV (Figure 4b) illustrate the likelihood of each unit to be active at a certain point during the day:

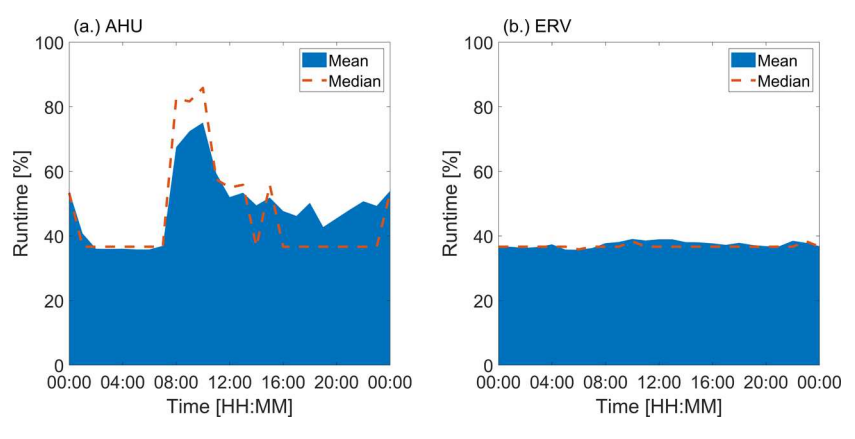


Figure 5. Mean and median diurnal runtime profiles for the Purdue ReNEWW House (a) AHU and (b) ERV.

$$Runtime_{AHU/ERV} (\%)$$

$$= \frac{time \ AHU/ERV \ are \ active}{total \ time \ (1 \ hour)} \times 100\%$$
(4)

Mean and median runtime profiles for each are shown in Figure 5. Here, the runtime is determined directly via the CT sensors and BEMS data 43,45 (in contrast to indirect approaches 105) and is calculated in hourly increments. The mean AHU runtime was the highest during the late morning, reaching 75% at around 10:00, and the lowest during the early morning, at around 36% from 02:00 to 07:00. The dramatic increase in the AHU runtime at 08:30 was due to the change in the floor 1 temperature set point. The AHU runtime was the lowest toward the end of the campaign due to a reduction in heating needs. The mean ERV runtime was 37% throughout the day; this was the same runtime as the AHU from 02:00 to 07:00 as modes 1 and 3 were active. Thus, for the ReNEWW House, the AHU runtime is governed by indoor air temperature oscillations and heating needs determined by the smart thermostats and the preset ERV cycle.

The runtime is a useful, but seldom measured, parameter for indoor air quality field campaigns that is valuable for inferring UFP source and loss processes associated with the highly variable duty cycles of residential HVAC systems. 20,45,46,105 The 24 h median AHU runtime at the ReNEWW House (36.7%) is within the range of median HVAC system runtimes for residences in heating-dominated climates during the heating season (35–45%), while longer than runtimes in cooling-dominated climates (20–27%). However, the AHU runtime is higher than that for a residence in Toronto, Canada (0–30%) that an outdoor air temperature of around 10 °C, due to the operation of the ERV which triggered the operation of the AHU when there was no call for heating (mode 3).

Linking BEMS, Smart Thermostat, and UFP Data During Indoor UFP Source Events. The integration of BEMS, smart thermostat, and UFP data collected in real time at the ReNEWW House can be seen in Figure 6, which shows an example indoor UFP source event for the electric induction cooktop (additional examples for other appliances are provided in Figures S18–S24). Shortly following the stepwise increase in the time-resolved cooktop power consumption profile (BEMS data, Figure 6a), the size-integrated UFP number concentration ($D_{\rm em}=10~{\rm to}~100~{\rm nm}$) sharply increases from background levels ($N<10^3~{\rm cm}^{-3}$) to $N\sim1~{\rm to}~2\times10^4~{\rm cm}^{-3}$ (SMPS data, Figure 6c). The short delay (<5 min) between the activation of the cooktop as indicated by the BEMS data and initiation of the UFP

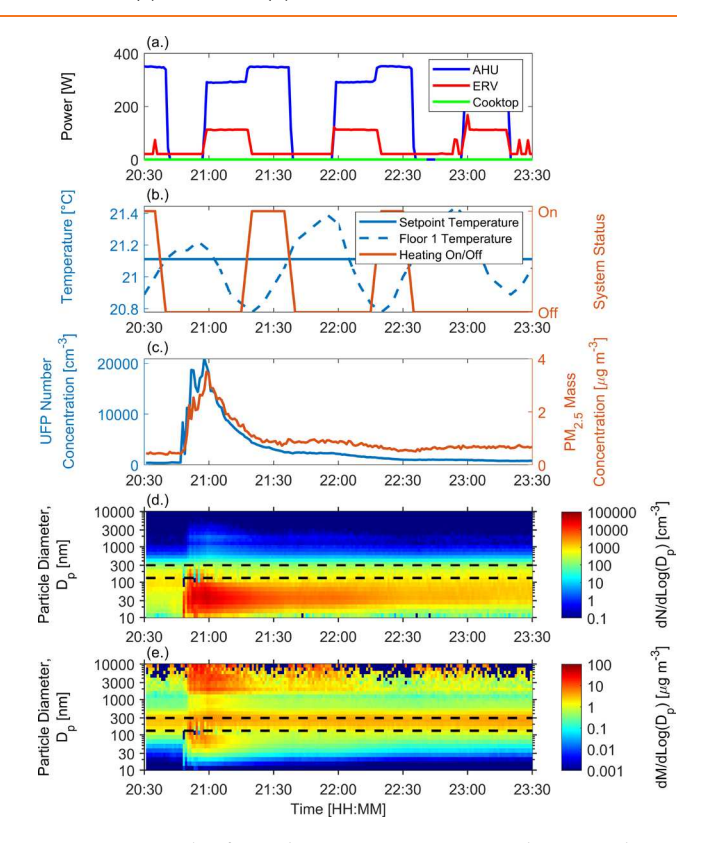


Figure 6. Example of an indoor UFP source event and associated UFP concentration elevation and decay at the Purdue ReNEWW House: (a) time-resolved power consumption profiles for the cooktop, AHU, and ERV as determined by BEMS data; (b) floor 1 set point and measured air temperatures and heating status as determined by smart thermostat data; (c) size-integrated UFP number concentration (10 to 100 nm) and $PM_{2.5}$ mass concentration (10 to 2500 nm, using size-resolved $ho_{
m eff}$ for cooking aerosol from Figure S5) the time series; (d) particle number size distribution $(dN/dlogD_p, cm^{-3})$ time series from 10 to 10 000 nm; and (e) particle mass size distribution ($dM/dlogD_p$, $\mu g m^{-3}$) time series from 10 to 10 000 nm (using size-resolved $\rho_{\rm eff}$ for cooking aerosol from Figure S5). The particle diameter (D_p) is defined as the electrical mobility diameter (D_{em}) from 10 to 300 nm (measured with SMPS) and optical diameter (Do) from 300 to 10 000 nm (measured with OPS). $D_{\rm em}$ = 150 to 300 nm was estimated through spline interpolation (indicated with dashed black lines).

concentration elevation was commonly observed. The delay is due in part to the time it takes for the cooking apparatus (e.g., pan, pot) and cooked items (e.g., oil, meat, vegetables) to reach

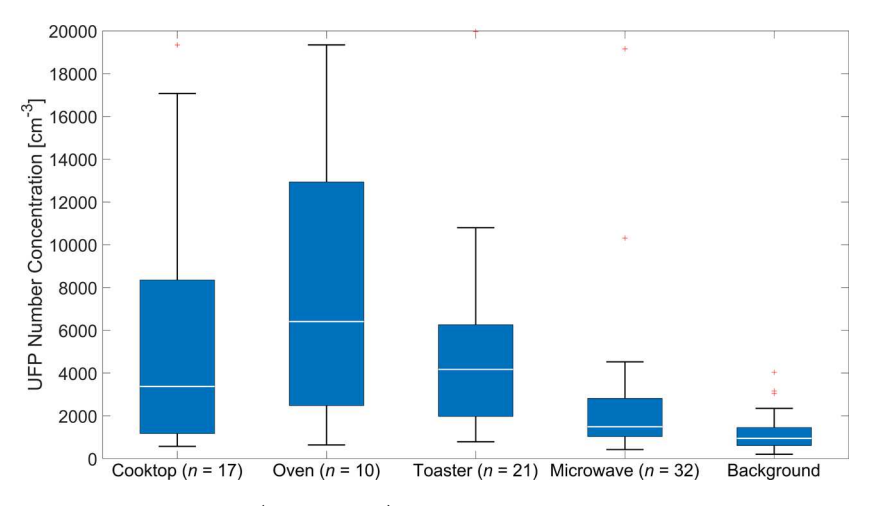


Figure 7. Size-integrated UFP number concentrations (10 to 100 nm) for indoor UFP source events identified for each electrical kitchen appliance as determined by BEMS data. UFP number concentrations during background periods in which no known indoor source was active at the Purdue ReNEWW House are shown for comparison. Box plots represent the interquartile range, whiskers represent the 5th and 95th percentiles, and markers represent outliers. Box plots include UFP number concentrations measured from the beginning of the source event until the UFP number concentration reached its maximum. *n* refers to source events when only one electrical kitchen appliance was active (Table 1).

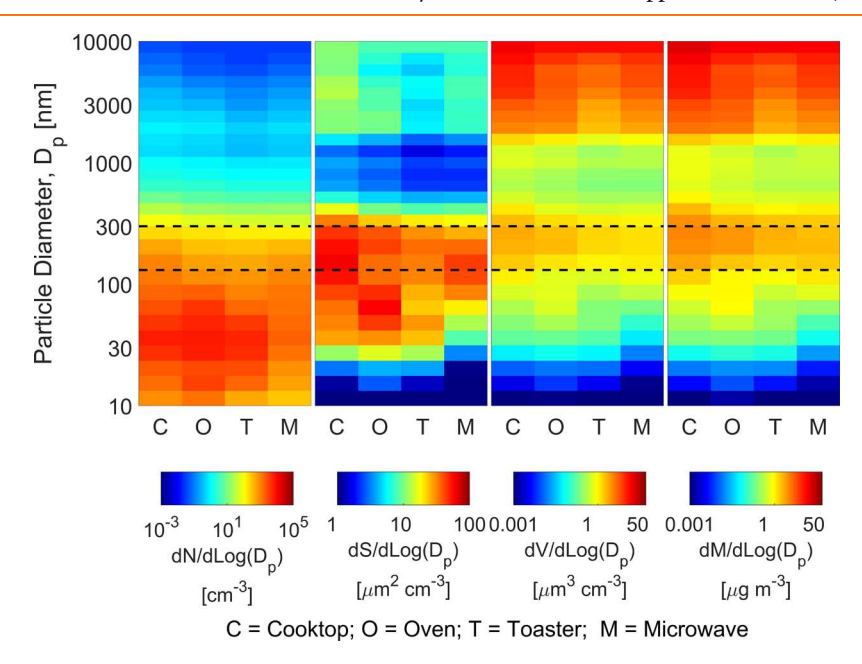


Figure 8. Median particle size distributions (10 to 10 000 nm) for indoor UFP source events identified for each electrical kitchen appliance as determined by BEMS data. The median particle size distributions include those measured from the beginning of the source event until the UFP number concentration reached its maximum. From left to right: particle number size distributions ($dN/dlogD_p$, $dlogD_p$,

temperatures sufficient for UFP production to occur (typically >100 °C), as documented in prior studies on heated cooking surfaces 81,82 and oils. 77,78 The maximum UFP number concentration is reached about 15 min after the cooktop is turned on. The period from the initial rise in UFP concentrations to the maximum concentration is used to compute the time-averaged UFP source rate ($S_{\rm KIT}$) following eq 2. The particle number and mass size distributions (Figure 6d,e) exhibit similar temporal trends during the source event, as does the size-integrated particle mass concentration ($PM_{2.5}$, $D_{\rm em(o)}=10$ to 2500 nm). The number size distributions

demonstrate that the majority of the particles produced (on a number basis) are in the UFP regime.

The UFP number concentration follows a near exponential decay after the cooking event (Figure 6c). It is this period that is used to estimate the total UFP loss rates (L) for each AHU/ERV operational mode. Figure 6a shows the power consumption profiles for the AHU and ERV taken from the BEMS data. Figure 6b shows the floor 1 heating status (on/off) and set point and measured air temperatures reported by the floor 1 smart thermostat. During the UFP decay, multiple AHU/ERV operational modes can be observed. From \sim 21:00 to 21:20, both the AHU and the ERV are active, while floor 1 heating is off

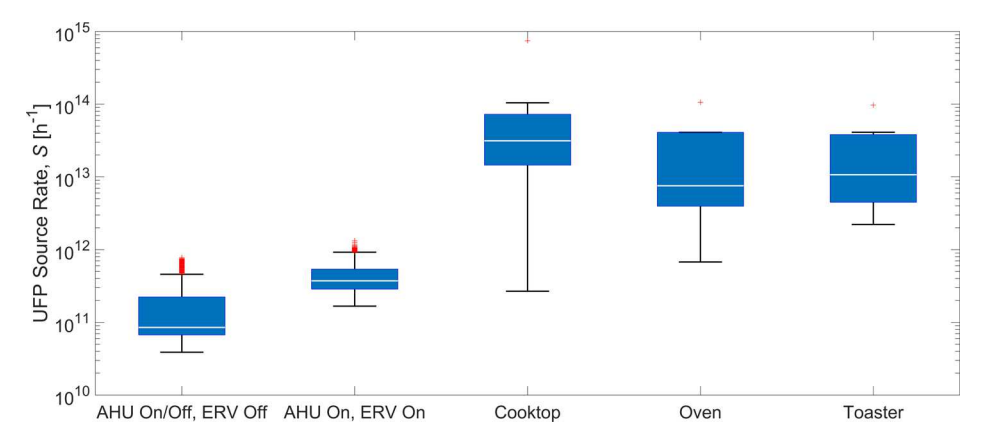


Figure 9. Size-integrated UFP source rates (*S*, 10 to 100 nm) for the operational modes of the AHU and ERV and indoor UFP source events identified for each electrical kitchen appliance as determined by BEMS data. AHU On/Off, ERV Off incorporates modes 1 and 2 and AHU On, ERV On incorporates modes 3 and 4 (Table 2). Box plots represent the interquartile range, whiskers represent the 5th and 95th percentiles, and markers represent outliers.

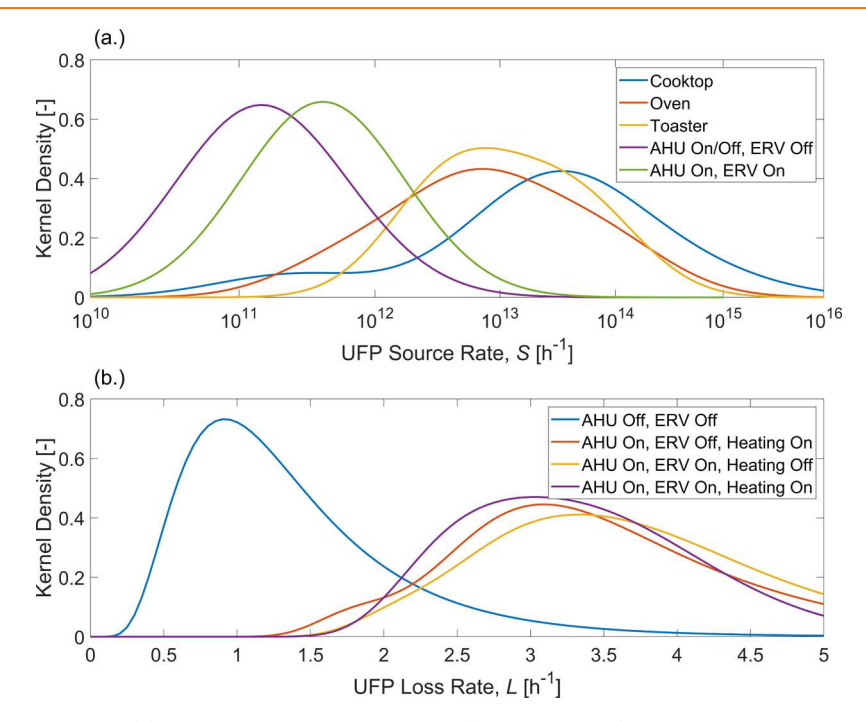


Figure 10. Kernel density functions for (a) size-integrated UFP source rates (*S*, 10 to 100 nm) for the operational modes of the AHU and ERV and indoor UFP source events identified for each electrical kitchen appliance as determined by BEMS data and (b) size-integrated total UFP loss rates (*L*, 10 to 100 nm) for the operational modes of the AHU and ERV as determined by BEMS data. For (a), AHU On/Off, ERV Off incorporates modes 1 and 2 and AHU On, ERV On incorporates modes 3 and 4 (Table 2).

(mode 3). From \sim 21:20 to 21:40, the AHU is on, the ERV is off, and floor 1 heating is on (mode 2—measured temperature falls 0.5 °F (0.28 °C) below the set point at \sim 21:20). From \sim 21:40 to 21:55, both the AHU and the ERV are off and heating is off (mode 1—measured temperature reaches the set point at \sim 21:40). As the AHU/ERV transitions from mode 1 to mode 3 at \sim 21:55, a slightly sharper decay is observed in the UFP data (Figure 6c), suggesting enhanced UFP removal associated with the operation of the AHU/ERV. Mode 4 was not observed during this period.

Electrical Kitchen Appliance-Resolved UFP Concentrations and Size Distributions. Electrical kitchen appliance-resolved UFP concentrations and size distributions are presented in Figures 7 and 8, respectively. UFP concentrations and size distributions were aggregated across all BEMS-

identified source events for which each appliance was active alone (Table 1). Figure 7 includes size-integrated UFP number concentrations (N, $D_{\rm em}$ = 10 to 100 nm), and Figure 8 includes measured number size distributions ($D_{\rm em(o)}$ = 10 to 10 000 nm) and their translation to surface area, volume, and mass. Multimodal log-normal fitting parameters are provided in Table S2 and Figures S8–S11 (appliance-resolved) and Table S3 and Figures S13–S17 (time-of-day-resolved). UFP number concentrations for background periods at the Purdue ReNEWW House during which no cooking occurred are shown for comparison in Figure 7 (median N = 9.5 × 10^2 cm⁻³).

The CT sensors and cloud-based BEMS provided a basis to partition the indoor UFP concentration and size distribution data set among different appliances. Such an approach can be useful for indoor UFP source apportionment 106 and can be

extended to real time measurements of other pollutants produced by cooking processes, such as volatile organic compounds. 12,107,108 The oven produced the highest UFP levels, with a median $N=6.4\times10^3$ cm⁻³, followed by the toaster and cooktop. A few source events for the oven and cooktop produced time-averaged $N>10^4$ cm⁻³. The microwave was not found to be a strong UFP emitter, elevating concentrations only slightly above background levels.

Variations in the magnitude of the particle number size distributions (Figures 8 and S7) were consistent with that observed for the UFP concentrations. For all appliances, UFPs dominated number size distributions. Across the entire campaign, UFPs ($D_{\rm em}$ = 10 to 100 nm) were found to contribute 80 to 94% (median of 86%) to total particle number concentrations ($D_{\rm em(o)}$ = 10 to 10 000 nm) (Figure S6). The prominent mode for the number size distributions was between $D_{\rm em} \sim$ 30 and 40 nm across the appliances, smaller than that observed during background periods ($D_{\rm em} \sim$ 70 nm). Surface area size distributions for the appliances were dominated by particles from $D_{\rm em} \sim$ 50 to 300 nm, whereas volume and mass size distributions were dominated by coarse mode particles ($D_{\rm o}$ > 2500 nm). The latter was likely produced due to both cooking emissions and floor dust resuspension. 9,11,73

Indoor UFP number concentrations at the ReNEWW House during cooking ($N \sim 10^3$ to 10^4 cm⁻³) and background ($N \sim 10^2$ to 10³ cm⁻³) periods are generally lower than those reported in prior studies (e.g., $N \sim 10^3$ to 10^6 cm⁻³). $^{11,14,16,74-76,79,106,109-118}$ Indoor UFP concentrations are context and location specific and depend on the dynamic relationship between S and L (eq 1). Notably, enhanced UFP removal at the Purdue ReNEWW House associated with the AHU and ERV (Figure 10b) may explain the lower UFP number concentrations, as does the positioning of the SMPS at a central location on floor 1 away from cooking emission plumes. Only one prior study 119 has reported on indoor UFPs in selected highperformance homes using electrical kitchen appliances with similar ventilation/infiltration attributes as the ReNEWW House. UFP concentrations during use of electric induction cooktops were similar to those reported here $(N \sim 10^3 \text{ cm}^{-3})$ and much less than those measured during the use of gas and electric resistance burners ($N \sim 10^5 \text{ cm}^{-3}$). 84,106,111,119

UFP Source Rates for Each Electrical Kitchen Appliance and AHU/ERV Operational Mode. The integration of BEMS, smart thermostat, and UFP data enable the estimation of size-integrated UFP source rates (S, $D_{\rm em}$ = 10 to 100 nm) for the electrical kitchen appliances and AHU/ERV. Figure 9 presents UFP source rates for the cooktop, oven, toaster, and merged AHU/ERV modes 1-2 (AHU on/off, ERV off) and 3-4 (AHU on, ERV on). Kernel density functions for each are provided in Figure 10a. Source rates were not estimated for the microwave since UFP concentrations increased marginally above the background (Figure 7). The UFP source rates are a generalizable output as they contextualize the measured UFP number concentrations (N) for the physical attributes of the indoor environment (L, V) in which they are measured (eq 1). 120 Thus, the use of the BEMS data to identify when different UFP sources are active and assign source rates during those periods is of value in better understanding the factors that increase UFP concentrations in smart homes.

UFP source rates for the electrical kitchen appliances were in the range of $S_{\rm KIT} \sim 10^{12}$ to $10^{14}\,h^{-1}$. Source rates for the cooktop were the highest (median $S_{\rm KIT} = 3.14 \times 10^{13}\,h^{-1}$) and exceeded $10^{14}\,h^{-1}$ for several cooking events. Source rates for the toaster

I

and oven were similar to one another, with median $S_{\rm KIT}=1.05\times 10^{13}\,{\rm h^{-1}}$ and $S_{\rm KIT}=7.55\times 10^{12}\,{\rm h^{-1}}$, respectively. Several cooking events for each resulted in $S_{\rm KIT}\sim 10^{14}\,{\rm h^{-1}}$. The Kernel density functions for the appliance-resolved UFP source rates illustrate the variability in the rate at which UFPs are emitted among the number of events identified with the BEMS data (Table 2). This variation is important to capture given the range of cooking temperatures, styles, and food types that can occur in a home with three occupants.

The estimated UFP source rates for the electrical kitchen appliances are generally consistent with those reported for cooking activities in prior studies (variable size ranges). Hussein et al. $(2006)^{16}$ reported a source rate of 3.6×10^{13} h⁻¹ for cooking activities in a home in Prague, Czech Republic; He et al. $(2004)^{117}$ reported median source rates of 4.4×10^{13} h⁻¹, 4.1×10^{13} h⁻¹, and 7.6×10^{12} h⁻¹ for stoves (gas and electric), toasting, and an oven, respectively, across 15 homes in Brisbane, Australia; Rim et al. $(2016)^{84}$ reported source rates of 1.08 to 1.68×10^{14} h⁻¹ for a heated electric resistance burner (no cooking and $D_{\rm em}$ down to 2 nm); and Zhao et al. $(2020)^{121}$ reported source rates for a range of cooking activities that were generally in the range of 1 to 5×10^{13} h⁻¹ across 40 homes in Germany.

UFP source rates for the AHU/ERV were significantly less than that for the electrical kitchen appliances, ranging from $S_{\rm AHU/ERV} \sim 10^{10}$ to $10^{12}~\rm h^{-1}$. The UFP source rate was greater when the ERV was on (modes 3–4, median $S_{\rm AHU/ERV} = 3.73 \times 10^{11}~\rm h^{-1}$) compared to when it was off (modes 1–2, median $S_{\rm AHU/ERV} = 8.51 \times 10^{10}~\rm h^{-1}$). The latter is strongly influenced by outdoor UFP penetration through the envelope of the ReNEWW House $^{88,91-93}$ (penetration factors were not calculated here). The ERV serves as an important interface between the indoor and outdoor atmospheres and continually draws in outdoor UFPs during its operation. As the outdoor air is directed from the ERV to the AHU, some UFPs are removed via deposition to AHU components (e.g., MERV 11 filter, heating/cooling coils, ducts); $^{8,89,90}_{\rm s}$ however, it is evident some fraction is still introduced to the occupied space.

While the AHU on/ERV on source rate (modes 3-4) was lower than that for cooking, the ERV is active much more frequently during the day (Figures 4 and 5, mean runtime of 37%) compared to the electrical kitchen appliances (Figure 2). The ERV can be viewed as a cyclical source of outdoor UFPs. This is important as the outdoor UFP number concentrations were typically higher than those measured indoors, especially during the weekdays, with indoor/outdoor (I/O) ratios often between 0.2 to 0.8 (Figure S6). For example, over a 24 h period, the ERV can deliver approximately 3.31×10^{12} UFPs indoors (S of $3.73 \times 10^{11} \, h^{-1} \times 0.37$ runtime fraction $\times 24 \, h$; assuming ERV contribution > AHU/infiltration). A typical cooktop event of 10 min (Table 1) would produce about 5.23×10^{12} UFPs (S of 3.14) $\times 10^{13} \,\mathrm{h^{-1}} \times 0.167 \,\mathrm{h}$). Therefore, it is necessary to consider the role of ERVs in modulating indoor UFP levels in energy-efficient homes such as NZEBs, where they are becoming more common.^{31,37} BEMS data is thus important in determining when and for how long the ERV acts as a UFP source.

UFP Loss Rates for Each AHU/ERV Operational Mode. Size-integrated total UFP loss rates ($L, D_{\rm em} = 10$ to 100 nm) for each for the four AHU/ERV operational modes (Table 2) are presented in Figure 10b as Kernel density functions. UFP loss rates are derived from the UFP number concentration decays following a source event and use the BEMS and smart thermostat data to partition the UFP data among the different

operational modes. The loss rates should be viewed as estimates of the overall rate of UFP removal from floor 1 of the ReNEWW House and are not apportioned by the various physical removal processes.

UFP loss rates vary among the four AHU/ERV operational modes, ranging from <0.5 to >4 h⁻¹. The width of the Kernel density functions reveal the variability in L for a given mode, demonstrating the probabilistic nature of UFP removal in homes. They are higher when the AHU and ERV are on (modes 2-4) compared to when they are both off (mode 1). During the latter, UFP sinks include indoor surface deposition, 2,85-87,122 exfiltration, 85,91 and interzonal air exchange 94 (assuming coagulation to be negligible for $N < 2 \times 10^4$ cm⁻³). 83,84 The mode 1 median $L = 1.18 \,\mathrm{h}^{-1}$ is consistent with prior estimates of size-integrated UFP loss rates for surface deposition by Wallace et al. $(2013)^{85}$ (median $L = 0.9 \text{ h}^{-1}$) and Stephens and Siegel $(2012)^{91}$ (median $L = 1.01 \text{ h}^{-1}$). Accelerated rates of UFP removal were periodically observed for mode 1 ($L > 1.5 \text{ h}^{-1}$). This may be due to temperature- and pressure-dependent variations in exfiltration and interzonal air exchange; 91,123 changing indoor airflow conditions, which affect the turbulent diffusion of UFPs to surfaces; 86,87 and enhanced thermophoretic deposition of UFPs to cooler surfaces for cooking emission plumes with higher temperatures. 124

The enhanced UFP removal associated with airflow through the AHU and ERV (modes 2-4) can be attributed to particle deposition to AHU components and ERV exhaust. UFP loss rates were similar among modes 2-4 and were generally in the range of L = 2.5 to $4 \, h^{-1}$ with median loss rates of $L = 3.33 \, h^{-1}$ for mode 2, $L = 3.54 \,\mathrm{h^{-1}}$ for mode 3, and $L = 3.30 \,\mathrm{h^{-1}}$ for mode 4. The ERV was likely responsible for the increase in L between modes 3 and 4 with mode 2 as the ratio of the ERV exhaust airflow rate to the floor 1 volume being 0.14 to 0.15 h^{-1} (Table S1). The similar Kernel density functions for L among modes 2– 4 suggest that the particle deposition to AHU components (e.g., MERV 11 filter, heating/cooling coils, ducts)^{8,89,90} is responsible for the majority of the UFP removal. A similar trend was observed by Stephens and Siegel (2013),6 whereby the activation of a residential HVAC system with a MERV 11 filter increased UFP loss rates by 1.3 to 1.7 h⁻¹ beyond the HVAC off

The net number of UFPs removed in a given period of time ($\int LNV \ dt$) is dependent on the duration over which the loss processes are active. Therefore, the effectiveness of the AHU/ERV in removing indoor UFPs is a function of not only their loss rates but also their respective runtimes (Figures 3–5). The AHU runtime is a significant factor in governing the effectiveness of an in-duct filter in removing indoor particles. Thus, BEMS-derived AHU/ERV runtimes are necessary for predicating indoor UFP number concentrations under different ventilation scenarios.

STUDY LIMITATIONS

Our study has several limitations. First, the spatial distribution in UFP concentrations throughout the ReNEWW House was not characterized with simultaneous sampling by multiple UFP sensors in different zones (e.g., basement, floor 1, outdoor air). Second, only overall UFP source and loss rates were reported and interzonal airflows under variable thermal and AHU/ERV operational conditions were not measured via tracer gas techniques given the complexity of conducting such measurements in occupied residences. Thus, the contribution of variable interzonal airflows to UFP source and loss rates is unknown. Third, the analysis of UFP source rates was only

focused on electrical kitchen appliances and the AHU/ERV. We were not able to identify nonelectrical sources with the BEMS data. However, the framework can be expanded to include other sensors (e.g., carbon dioxide sensors, motion sensors, window sensors, etc.) to better characterize indoor activities and their impact on UFP dynamics.

■ ENGINEERING SIGNIFICANCE

This study introduced a new data-driven framework for using building energy and smart thermostat data to characterize the dynamics of sub-100 nm UFPs in an occupied net-zero energy home equipped with a comprehensive sensing and data management system. The framework provides a basis for automated detection of indoor air pollution source events associated with the use of electrical kitchen appliances for cooking. As illustrated in this study, residential HVAC systems (AHUs/ERVs) serve as both a source and a sink for UFPs. CT sensors, BEMS, and smart thermostats can be used together to evaluate the transient operational modes and runtimes of HVAC systems. This enables assessment of how HVAC systems modulate indoor air pollutant concentrations. The approach presented here can inform smart ventilation control strategies ^{17,19,21} that can be used to regulate the operation of AHUs and ERVs based on outdoor pollution levels and the activation of indoor sources. Such strategies are needed given the growing chemistry^{3,125} and the impact of UFPs on human health and well-being. 52,54,56,59,60

This study demonstrates the importance of applying a systems-level approach to indoor air quality field measurements as building systems and occupant activities are responsible for driving significant changes in indoor particle concentrations. The ReNEWW House BEMS can tell us the real time status of the HVAC system and if an occupant is cooking and use this collective information to explain fluctuations in indoor UFP levels. Lastly, the framework can be used to predict UFP concentrations under different scenarios by coupling the estimated UFP source and loss rates with the energy use profiles for the electrical kitchen appliances and AHU/ERV.

ASSOCIATED CONTENT

Supporting Information

The Supporting Information is available free of charge at https://pubs.acs.org/doi/10.1021/acsestengg.1c00002.

Additional results regarding volumetric airflow rates for the AHU and ERV; multimodal log-normal fitting parameters for the particle number, surface area, volume, and mass size distributions; outdoor UFP number concentrations; measured size-resolved particle effective densities; and photos of the Purdue ReNEWW House (PDF)

AUTHOR INFORMATION

Corresponding Author

Brandon E. Boor — Lyles School of Civil Engineering and Ray W. Herrick Laboratories, Center for High Performance Buildings, Purdue University, West Lafayette, Indiana 47907, United States; orcid.org/0000-0003-1011-4100; Email: bboor@purdue.edu

Authors

Jinglin Jiang — Lyles School of Civil Engineering and Ray W. Herrick Laboratories, Center for High Performance Buildings, Purdue University, West Lafayette, Indiana 47907, United States

Nusrat Jung — Lyles School of Civil Engineering and Ray W. Herrick Laboratories, Center for High Performance Buildings, Purdue University, West Lafayette, Indiana 47907, United States; © orcid.org/0000-0002-8874-8923

Complete contact information is available at: https://pubs.acs.org/10.1021/acsestengg.1c00002

Notes

The authors declare no competing financial interest.

ACKNOWLEDGMENTS

Financial support was provided by the National Science Foundation (CBET-1847493) and the Purdue University Instructional Innovation Program. The authors thank the residents of the Purdue ReNEWW House and Jason Schneemann of Whirlpool Corporation for their help and support and Dr. Tianren Wu (Purdue University) for conducting the particle effective density measurements.

REFERENCES

- (1) Riley, W. J.; McKone, T. E.; Lai, A. C. K.; Nazaroff, W. W. Indoor Particulate Matter of Outdoor Origin: Importance of Size-Dependent Removal Mechanisms. *Environ. Sci. Technol.* **2002**, *36* (2), 200–207.
- (2) Nazaroff, W. W. Indoor Particle Dynamics. Indoor Air 2004, 14,
- (3) Goldstein, A. H.; Nazaroff, W. W.; Weschler, C. J.; Williams, J. How Do Indoor Environments Affect Air Pollution Exposure? *Environ. Sci. Technol.* **2020**, *SS*, 100–108.
- (4) Klepeis, N. E.; Nelson, W. C.; Ott, W. R.; Robinson, J. P.; Tsang, A. M.; Switzer, P.; Behar, J. v.; Hern, S. C.; Engelmann, W. H. The National Human Activity Pattern Survey (NHAPS): A Resource for Assessing Exposure to Environmental Pollutants. *J. Exposure Sci. Environ. Epidemiol.* 2001, 11 (3), 231–252.
- (5) Alavy, M.; Siegel, J. A. In-situ Effectiveness of Residential HVAC Filters. *Indoor Air* **2020**, 30 (1), 156–166.
- (6) Stephens, B.; Siegel, J. A. Ultrafine Particle Removal by Residential Heating, Ventilating, and Air-Conditioning Filters. *Indoor Air* **2013**, 23 (6), 488–497.
- (7) Howard-Reed, C.; Wallace, L. A.; Emmerich, S. J. Effect of Ventilation Systems and Air Filters on Decay Rates of Particles Produced by Indoor Sources in an Occupied Townhouse. *Atmos. Environ.* **2003**, *37*, 5295–5306.
- (8) Stephens, B.; Siegel, J. A. Comparison of Test Methods for Determining the Particle Removal Efficiency of Filters in Residential and Light-Commercial Central HVAC Systems. *Aerosol Sci. Technol.* **2012**, *46* (5), 504–513.
- (9) Tian, Y.; Arata, C.; Boedicker, E.; Lunderberg, D. M.; Patel, S.; Sankhyan, S.; Kristensen, K.; Misztal, P. K.; Farmer, D. K.; Vance, M.; Novoselac, A.; Nazaroff, W. W.; Goldstein, A. H. Indoor Emissions of Total and Fluorescent Supermicron Particles during HOMEChem. *Indoor Air* 2020, 88–98.
- (10) Farmer, D. K.; Vance, M. E.; Abbatt, J. P. D.; Abeleira, A.; Alves, M. R.; Arata, C.; Boedicker, E.; Bourne, S.; Cardoso-Saldaña, F.; Corsi, R.; Decarlo, P. F.; Goldstein, A. H.; Grassian, V. H.; Hildebrandt Ruiz, L.; Jimenez, J. L.; Kahan, T. F.; Katz, E. F.; Mattila, J. M.; Nazaroff, W. W.; Novoselac, A.; O'Brien, R. E.; Or, V. W.; Patel, S.; Sankhyan, S.; Stevens, P. S.; Tian, Y.; Wade, M.; Wang, C.; Zhou, S.; Zhou, Y. Overview of HOMEChem: House Observations of Microbial and Environmental Chemistry. *Environmental Science: Processes and Impacts* 2019, 21 (8), 1280–1300.

- (11) Patel, S.; Sankhyan, S.; Boedicker, E. K.; Decarlo, P. F.; Farmer, D. K.; Goldstein, A. H.; Katz, E. F.; Nazaroff, W. W.; Tian, Y.; Vanhanen, J.; Vance, M. E. Indoor Particulate Matter during HOMEChem: Concentrations, Size Distributions, and Exposures. *Environ. Sci. Technol.* **2020**, *54* (12), 7107–7116.
- (12) Liu, Y.; Misztal, P. K.; Xiong, J.; Tian, Y.; Arata, C.; Weber, R. J.; Nazaroff, W. W.; Goldstein, A. H. Characterizing Sources and Emissions of Volatile Organic Compounds in a Northern California Residence Using Space- and Time-Resolved Measurements. *Indoor Air* **2019**, 29 (4), 630–644.
- (13) Militello-Hourigan, R. E.; Miller, S. L. The Impacts of Cooking and an Assessment of Indoor Air Quality in Colorado Passive and Tightly Constructed Homes. *Building and Environment* **2018**, *144*, 573–582.
- (14) Hussein, T.; Hämeri, K.; Heikkinen, M. S. A.; Kulmala, M. Indoor and Outdoor Particle Size Characterization at a Family House in Espoo-Finland. *Atmos. Environ.* **2005**, *39* (20), 3697–3709.
- (15) Hussein, T.; Korhonen, H.; Herrmann, E.; Hämeri, K.; Lehtinen, K. E. J.; Kulmala, M. Emission Rates Due to Indoor Activities: Indoor Aerosol Model Development, Evaluation, and Applications. *Aerosol Sci. Technol.* **2005**, 39 (11), 1111–1127.
- (16) Hussein, T.; Glytsos, T.; Ondráček, J.; Dohányosová, P.; Ždímal, V.; Hämeri, K.; Lazaridis, M.; Smolík, J.; Kulmala, M. Particle Size Characterization and Emission Rates during Indoor Activities in a House. *Atmos. Environ.* **2006**, *40* (23), 4285–4307.
- (17) Froufe, M. M.; Chinelli, C. K.; Guedes, A. L. A.; Haddad, A. N.; Hammad, A. W. A.; Soares, C. A. P. Smart Buildings: Systems and Drivers. *Buildings* **2020**, *10* (9), 153.
- (18) Cetin, K. S.; O'Neill, Z. Smart Meters and Smart Devices in Buildings: A Review of Recent Progress and Influence on Electricity Use and Peak Demand. *Current Sustainable/Renewable Energy Reports* **2017**, *4* (1), 1–7.
- (19) Schieweck, A.; Uhde, E.; Salthammer, T.; Salthammer, L. C.; Morawska, L.; Mazaheri, M.; Kumar, P. Smart Homes and the Control of Indoor Air Quality. *Renewable Sustainable Energy Rev.* **2018**, *94*, 705–718.
- (20) Touchie, M. F.; Siegel, J. A. Residential HVAC Runtime from Smart Thermostats: Characterization, Comparison, and Impacts. *Indoor Air* **2018**, 28 (6), 905–915.
- (21) Guyot, G.; Sherman, M. H.; Walker, I. S. Smart Ventilation Energy and Indoor Air Quality Performance in Residential Buildings: A Review. *Energy and Buildings* **2018**, *165*, 416–430.
- (22) Stopps, H.; Touchie, M. F. Managing Thermal Comfort in Contemporary High-Rise Residential Buildings: Using Smart Thermostats and Surveys to Identify Energy Efficiency and Comfort Opportunities. *Building and Environment* **2020**, *173*, 106748.
- (23) Batek, A.; Aliprantis, D. Improving Home Appliance Energy Use Scheduling: Insights from a Remodeled, Energy Efficient Home. In 2016 IEEE Power and Energy Society Innovative Smart Grid Technologies Conference, ISGT 2016; Institute of Electrical and Electronics Engineers Inc.: 2016, DOI: 10.1109/ISGT.2016.7781253.
- (24) Ock, J.; Issa, R. R. A.; Flood, I. Smart Building Energy Management Systems (BEMS) Simulation Conceptual Framework. In *Proceedings Winter Simulation Conference*; IEEE: 2016; pp 3237—3245, DOI: 10.1109/WSC.2016.7822355.
- (25) Minoli, D.; Sohraby, K.; Occhiogrosso, B. IoT Considerations, Requirements, and Architectures for Smart Buildings-Energy Optimization and Next-Generation Building Management Systems. *IEEE Internet Things J.* **2017**, 4 (1), 269–283.
- (26) Akkaya, K.; Guvenc, I.; Aygun, R.; Pala, N.; Kadri, A. IoT-Based Occupancy Monitoring Techniques for Energy-Efficient Smart Buildings. In 2015 IEEE Wireless Communications and Networking Conference Workshops, WCNCW 2015; Institute of Electrical and Electronics Engineers Inc.: 2015; pp 58–63, DOI: 10.1109/WCNCW.2015.7122529.
- (27) Bashir, M. R.; Gill, A. Q. IoT Enabled Smart Buildings: A Systematic Review. In 2017 Intelligent Systems Conference, IntelliSys 2017; Institute of Electrical and Electronics Engineers Inc.: 2018; pp 151–159, DOI: 10.1109/IntelliSys.2017.8324283.

- (28) Vares, S.; Häkkinen, T.; Ketomäki, J.; Shemeikka, J.; Jung, N. Impact of Renewable Energy Technologies on the Embodied and Operational GHG Emissions of a Nearly Zero Energy Building. *Journal of Building Engineering* **2019**, 22, 439–450.
- (29) Jung, N.; Paiho, S.; Shemeikka, J.; Lahdelma, R.; Airaksinen, M. Energy Performance Analysis of an Office Building in Three Climate Zones. *Energy and Buildings* **2018**, *158*, 1023–1035.
- (30) Jung, N.; Moula, M. E.; Fang, T.; Hamdy, M.; Lahdelma, R. Social Acceptance of Renewable Energy Technologies for Buildings in the Helsinki Metropolitan Area of Finland. *Renewable Energy* **2016**, *99*, 813–824
- (31) Wu, W.; Skye, H. M. Net-Zero Nation: HVAC and PV Systems for Residential Net-Zero Energy Buildings across the United States. *Energy Convers. Manage.* **2018**, 177, 605–628.
- (32) Ng, L. C.; Payne, W. V. Energy Use Consequences of Ventilating a Net-Zero Energy House. *Appl. Therm. Eng.* **2016**, *96*, 151–160.
- (33) Ng, L.; Poppendieck, D.; Dols, W. S.; Dougherty, B. P.; Emmerich, S. J. NIST Net-Zero Energy Residential Test Facility. *ASHRAE Journal* **2018**, 12–19.
- (34) Zeiler, W.; Boxem, G. Net-Zero Energy Building Schools. *Renewable Energy* **2013**, 49, 282–286.
- (35) Caskey, S. L.; Bowler, E. J.; Groll, E. A. Analysis on a Net-Zero Energy Renovation of a 1920s Vintage Home. *Science and Technology for the Built Environment* **2016**, 22 (7), 1060–1073.
- (36) Hunter Fanney, A.; Healy, W.; Payne, V.; Kneifel, J.; Ng, L.; Dougherty, B.; Ullah, T.; Omar, F. Small Changes Yield Large Results at NIST's Net-Zero Energy Residential Test Facility. *J. Sol. Energy Eng.* **2017**, 139 (6), 061009.
- (37) Wu, W.; Skye, H. M.; Domanski, P. A. Selecting HVAC Systems to Achieve Comfortable and Cost-Effective Residential Net-Zero Energy Buildings. *Appl. Energy* **2018**, *212*, 577–591.
- (38) Poppendieck, D. G.; Ng, L. C.; Persily, A. K.; Hodgson, A. T. Long Term Air Quality Monitoring in a Net-Zero Energy Residence Designed with Low Emitting Interior Products. *Building and Environment* 2015, 94 (P1), 33–42.
- (39) Ng, L.; Poppendieck, D.; Dols, W. S.; Emmerich, S. J. Evaluating Indoor Air Quality and Energy Impacts of Ventilation in a Net-Zero Energy House Using a Coupled Model. *Science and Technology for the Built Environment* **2018**, 24 (2), 124–134.
- (40) Langer, S.; Bekö, G.; Bloom, E.; Widheden, A.; Ekberg, L. Indoor Air Quality in Passive and Conventional New Houses in Sweden. *Building and Environment* **2015**, *93* (P1), 92–100.
- (41) Szirtesi, K.; Angyal, A.; Szoboszlai, Z.; Furu, E.; Török, Z.; Igaz, T.; Kertész, Z. Airborne Particulate Matter: An Investigation of Buildings with Passive House Technology in Hungary. *Aerosol Air Qual. Res.* **2018**, *18* (5), 1282–1293.
- (42) Caskey, S. L.; Groll, E. A. Hybrid Air-Hydronic HVAC Performance in a Residential Net-Zero Energy Retrofit. *Energy and Buildings* **2018**, *158*, 342–355.
- (43) Cetin, K. S.; Novoselac, A. Single and Multi-Family Residential Central All-Air HVAC System Operational Characteristics in Cooling-Dominated Climate. *Energy and Buildings* **2015**, *96*, 210–220.
- (44) Cetin, K. S.; Tabares-Velasco, P. C.; Novoselac, A. Appliance Daily Energy Use in New Residential Buildings: Use Profiles and Variation in Time-of-Use. *Energy and Buildings* **2014**, *84*, 716–726.
- (45) Stephens, B.; Siegel, J. A.; Novoselac, A. Operational Characteristics of Residential and Light-Commercial Air-Conditioning Systems in a Hot and Humid Climate Zone. *Building and Environment* **2011**, 46 (10), 1972–1983.
- (46) Li, T.; Alavy, M.; Siegel, J. A. Measurement of Residential HVAC System Runtime. *Building and Environment* **2019**, *150*, 99–107.
- (47) Oberdörster, G.; Šharp, Z.; Atudorei, V.; Elder, A.; Gelein, R.; Kreyling, W.; Cox, C. Translocation of Inhaled Ultrafine Particles to the Brain. *Inhalation Toxicol.* **2004**, *16*, 437–445.
- (48) Oberdörster, G.; Oberdörster, E.; Oberdörster, J. Nanotoxicology: An Emerging Discipline Evolving from Studies of Ultrafine Particles. *Environ. Health Perspect.* **2005**, 823–839.
- (49) Stone, V.; Miller, M. R.; Clift, M. J. D.; Elder, A.; Mills, N. L.; Møller, P.; Schins, R. P. F.; Vogel, U.; Kreyling, W. G.; Jensen, K. A.;

- Kuhlbusch, T. A. J.; Schwarze, P. E.; Hoet, P.; Pietroiusti, A.; de Vizcaya-Ruiz, A.; Baeza-Squiban, A.; Teixeira, J. P.; Tran, C. L.; Cassee, F. R. Nanomaterials versus Ambient Ultrafine Particles: An Opportunity to Exchange Toxicology Knowledge. *Environmental Health Perspectives* **2017**, 106002.
- (50) Sioutas, C.; Delfino, R. J.; Singh, M. Exposure Assessment for Atmospheric Ultrafine Particles (UFPs) and Implications in Epidemiologic Research. *Environ. Health Perspect.* **2005**, 947–955.
- (51) Baldauf, R. W.; Devlin, R. B.; Gehr, P.; Giannelli, R.; Hassett-Sipple, B.; Jung, H.; Martini, G.; McDonald, J.; Sacks, J. D.; Walker, K. Ultrafine Particle Metrics and Research Considerations: Review of the 2015 UFP Workshop. In *International Journal of Environmental Research and Public Health*; MDPI AG: 2016; Vol. 13, DOI: 10.3390/ijerph13111054.
- (52) Li, N.; Georas, S.; Alexis, N.; Fritz, P.; Xia, T.; Williams, M. A.; Horner, E.; Nel, A. A Work Group Report on Ultrafine Particles (American Academy of Allergy, Asthma & Immunology): Why Ambient Ultrafine and Engineered Nanoparticles Should Receive Special Attention for Possible Adverse Health Outcomes in Human Subjects. *J. Allergy Clin. Immunol.* **2016**, *138* (2), 386–396.
- (53) Li, R.; Yang, J.; Saffari, A.; Jacobs, J.; Baek, K. I.; Hough, G.; Larauche, M. H.; Ma, J.; Jen, N.; Moussaoui, N.; Zhou, B.; Kang, H.; Reddy, S.; Henning, S. M.; Campen, M. J.; Pisegna, J.; Li, Z.; Fogelman, A. M.; Sioutas, C.; Navab, M.; Hsiai, T. K. Ambient Ultrafine Particle Ingestion Alters Gut Microbiota in Association with Increased Atherogenic Lipid Metabolites. *Sci. Rep.* **2017**, *7*, 42906.
- (54) Delfino, R. J.; Sioutas, C.; Malik, S. Potential Role of Ultrafine Particles in Associations between Airborne Particle Mass and Cardiovascular Health. *Environ. Health Perspect.* **2005**, *113*, 934–946.
- (55) Pietropaoli, A. P.; Frampton, M. W.; Hyde, R. W.; Morrow, P. E.; Oberdörster, G.; Cox, C.; Speers, D. M.; Frasier, L. M.; Chalupa, D. C.; Huang, L. S.; Utell, M. J. Pulmonary Function, Diffusing Capacity, and Inflammation in Healthy and Asthmatic Subjects Exposed to Ultrafine Particles. *Inhalation Toxicol.* **2004**, *16*, 59–72.
- (56) Chen, K.; Schneider, A.; Cyrys, J.; Wolf, K.; Meisinger, C.; Heier, M.; von Scheidt, W.; Kuch, B.; Pitz, M.; Peters, A.; Breitner, S. Hourly Exposure to Ultrafine Particle Metrics and the Onset of Myocardial Infarction in Augsburg, Germany. *Environ. Health Perspect.* **2020**, *128* (1), 017003.
- (57) Allen, J. L.; Oberdorster, G.; Morris-Schaffer, K.; Wong, C.; Klocke, C.; Sobolewski, M.; Conrad, K.; Mayer-Proschel, M.; Cory-Slechta, D. A. Developmental Neurotoxicity of Inhaled Ambient Ultrafine Particle Air Pollution: Parallels with Neuropathological and Behavioral Features of Autism and Other Neurodevelopmental Disorders. *NeuroToxicology* **2017**, *59*, 140–154.
- (58) Olsen, Y.; Karottki, D. G.; Jensen, D. M.; Bekö, G.; Kjeldsen, B. U.; Clausen, G.; Hersoug, L. G.; Holst, G. J.; Wierzbicka, A.; Sigsgaard, T.; Linneberg, A.; Møller, P.; Loft, S. Vascular and Lung Function Related to Ultrafine and Fine Particles Exposure Assessed by Personal and Indoor Monitoring: A Cross-Sectional Study. *Environ. Health* **2014**, *13* (1), 112.
- (59) Downward, G. S.; van Nunen, E. J. H. M.; Kerckhoffs, J.; Vineis, P.; Brunekreef, B.; Boer, J. M. A.; Messier, K. P.; Roy, A.; Verschuren, W. M. M.; van der Schouw, Y. T.; Sluijs, I.; Gulliver, J.; Hoek, G.; Vermeulen, R. Long-Term Exposure to Ultrafine Particles and Incidence of Cardiovascular and Cerebrovascular Disease in a Prospective Study of a Dutch Cohort. *Environ. Health Perspect.* **2018**, 126 (12), 127007.
- (60) Pieters, N.; Koppen, G.; van Poppel, M.; de Prins, S.; Cox, B.; Dons, E.; Nelen, V.; Panis, L. I.; Plusquin, M.; Schoeters, G.; Nawrot, T. S. Blood Pressure and Same-Day Exposure to Air Pollution at School: Associations with Nano-Sized to Coarse PM in Children. *Environ. Health Perspect.* **2015**, 123 (7), 737–742.
- (61) Salehi, M.; Odimayomi, T.; Ra, K.; Ley, C.; Julien, R.; Nejadhashemi, A. P.; Hernandez-Suarez, J. S.; Mitchell, J.; Shah, A. D.; Whelton, A. An Investigation of Spatial and Temporal Drinking Water Quality Variation in Green Residential Plumbing. *Building and Environment* **2020**, *169*, 106566.

- (62) Yamada, M.; Takaya, M.; Ogura, I. Performance Evaluation of Newly Developed Portable Aerosol Sizers Used for Nanomaterial Aerosol Measurements. *Ind. Health* **2015**, *53* (6), 511–516.
- (63) Vo, E.; Horvatin, M.; Zhuang, Z. Performance Comparison of Field Portable Instruments to the Scanning Mobility Particle Sizer Using Monodispersed and Polydispersed Sodium Chloride Aerosols. *Annals of Work Exposures and Health* **2018**, 62 (6), 711–720.
- (64) Fonseca, A. S.; Viana, M.; Pérez, N.; Alastuey, A.; Querol, X.; Kaminski, H.; Todea, A. M.; Monz, C.; Asbach, C. Intercomparison of a Portable and Two Stationary Mobility Particle Sizers for Nanoscale Aerosol Measurements. *Aerosol Sci. Technol.* **2016**, *50* (7), 653–668.
- (65) Hsiao, T. C.; Lee, Y. C.; Chen, K. C.; Ye, W. C.; Sopajaree, K.; Tsai, Y. I. Experimental Comparison of Two Portable and Real-Time Size Distribution Analyzers for Nano/Submicron Aerosol Measurements. *Aerosol Air Qual. Res.* **2016**, *16* (4), 919–929.
- (66) Wu, T.; Boor, B. E. Characterization of a Thermal Aerosol Generator for HVAC Filtration Experiments (RP-1734). *Science and Technology for the Built Environment* **2020**, 26 (6), 816–834.
- (67) Seinfeld, J. H.; Pandis, S. N. Atmospheric Chemistry and Physics: From Air Pollution to Climate Change, 3rd ed.; Wiley: 2016.
- (68) Wu, T.; Boor, B. E. Urban Aerosol Size Distributions: A Global Perspective. *Atmospheric Chemistry & Physics Discussions* **2020**, DOI: 10.5194/acp-2020-92.
- (69) Poon, C.; Wallace, L.; Lai, A. C. K. Experimental Study of Exposure to Cooking Emitted Particles under Single Zone and Two-Zone Environments. *Building and Environment* **2016**, *104*, 122–130.
- (70) Zhou, J.; Fang, W.; Cao, Q.; Yang, L.; Chang, V. W. C.; Nazaroff, W. W. Influence of Moisturizer and Relative Humidity on Human Emissions of Fluorescent Biological Aerosol Particles. *Indoor Air* **2017**, 27 (3), 587–598.
- (71) Tian, Y.; Liu, Y.; Misztal, P. K.; Xiong, J.; Arata, C. M.; Goldstein, A. H.; Nazaroff, W. W. Fluorescent Biological Aerosol Particles: Concentrations, Emissions, and Exposures in a Northern California Residence. *Indoor Air* **2018**, *28* (4), 559–571.
- (72) Yang, S.; Bekö, G.; Wargocki, P.; Williams, J.; Licina, D. Human Emissions of Size-Resolved Fluorescent Aerosol Particles: Influence of Personal and Environmental Factors. *Environ. Sci. Technol.* **2020**, 509–518
- (73) Wu, T.; Täubel, M.; Holopainen, R.; Viitanen, A. K.; Vainiotalo, S.; Tuomi, T.; Keskinen, J.; Hyvärinen, A.; Hämeri, K.; Saari, S. E.; Boor, B. E. Infant and Adult Inhalation Exposure to Resuspended Biological Particulate Matter. *Environ. Sci. Technol.* **2018**, *52* (1), 237–247.
- (74) Wan, M. P.; Wu, C. L.; Sze To, G. N.; Chan, T. C.; Chao, C. Y. H. Ultrafine Particles, and PM2.5 Generated from Cooking in Homes. *Atmos. Environ.* **2011**, *45* (34), 6141–6148.
- (75) Buonanno, G.; Morawska, L.; Stabile, L. Particle Emission Factors during Cooking Activities. *Atmos. Environ.* **2009**, 43 (20), 3235–3242.
- (76) Yeung, L. L.; To, W. M. Size Distributions of the Aerosols Emitted from Commercial Cooking Processes. *Indoor Built Environ.* **2008**, *17* (3), 220–229.
- (77) Amouei Torkmahalleh, M.; Zhao, Y.; Hopke, P. K.; Rossner, A.; Ferro, A. R. Additive Impacts on Particle Emissions from Heating Low Emitting Cooking Oils. *Atmos. Environ.* **2013**, *74*, 194–198.
- (78) Torkmahalleh, M. A.; Goldasteh, I.; Zhao, Y.; Udochu, N. M.; Rossner, A.; Hopke, P. K.; Ferro, A. R. PM 2.5 and Ultrafine Particles Emitted during Heating of Commercial Cooking Oils. *Indoor Air* **2012**, 22 (6), 483–491.
- (79) Zhang, Q.; Gangupomu, R. H.; Ramirez, D.; Zhu, Y. Measurement of Ultrafine Particles and Other Air Pollutants Emitted by Cooking Activities. *Int. J. Environ. Res. Public Health* **2010**, 7 (4), 1744–1759.
- (80) Jørgensen, R. B.; Strandberg, B.; Sjaastad, A. K.; Johansen, A.; Svendsen, K. Simulated Restaurant Cook Exposure to Emissions of PAHs, Mutagenic Aldehydes, and Particles from Frying Bacon. *J. Occup. Environ. Hyg.* **2013**, *10* (3), 122–131.
- (81) Wallace, L. A.; Ott, W. R.; Weschler, C. J. Ultrafine Particles from Electric Appliances and Cooking Pans: Experiments Suggesting

- Desorption/Nucleation of Sorbed Organics as the Primary Source. *Indoor Air* **2015**, 25 (5), 536–546.
- (82) Wallace, L. A.; Ott, W. R.; Weschler, C. J.; Lai, A. C. K. Desorption of SVOCs from Heated Surfaces in the Form of Ultrafine Particles. *Environ. Sci. Technol.* **2017**, *51* (3), 1140–1146.
- (83) Wallace, L.; Jeong, S. G.; Rim, D. Dynamic Behavior of Indoor Ultrafine Particles (2.3–64 Nm) Due to Burning Candles in a Residence. *Indoor Air* **2019**, *29* (6), 1018–1027.
- (84) Rim, D.; Choi, J.; Wallace, L. A. Size-Resolved Source Emission Rates of Indoor Ultrafine Particles Considering Coagulation. *Environ. Sci. Technol.* **2016**, *50* (18), 10031–10038.
- (85) Wallace, L.; Kindzierski, W.; Kearney, J.; MacNeill, M.; Héroux, M. E.; Wheeler, A. J. Fine and Ultrafine Particle Decay Rates in Multiple Homes. *Environ. Sci. Technol.* **2013**, *47* (22), 12929–12937.
- (86) Lai, A. C. K.; Nazaroff, W. W. Modeling Indoor Particle Deposition from Turbulent Flow onto Smooth Surfaces. *J. Aerosol Sci.* **2000**, *31* (4), 463–476.
- (87) Thatcher, T. L.; Lai, A. C. K.; Moreno-Jackson, R.; Sextro, R. G.; Nazaroff, W. W. Effects of Room Furnishings and Air Speed on Particle Deposition Rates Indoors. *Atmos. Environ.* **2002**, *36*, 1811–1819.
- (88) Chao, C. Y. H.; Wan, M. P.; Cheng, E. C. K. Penetration Coefficient and Deposition Rate as a Function of Particle Size in Non-Smoking Naturally Ventilated Residences. *Atmos. Environ.* **2003**, *37* (30), 4233–4241.
- (89) Singer, B. C.; Delp, W. W.; Black, D. R.; Walker, I. S. Measured Performance of Filtration and Ventilation Systems for Fine and Ultrafine Particles and Ozone in an Unoccupied Modern California House. *Indoor Air* **2017**, 27 (4), 780–790.
- (90) Waring, M. S.; Siegel, J. A. Particle Loading Rates for HVAC Filters, Heat Exchangers, and Ducts. *Indoor Air* **2008**, *18* (3), 209–224.
- (91) Stephens, B.; Siegel, J. A. Penetration of Ambient Submicron Particles into Single-Family Residences and Associations with Building Characteristics. *Indoor Air* **2012**, 22 (6), 501–513.
- (92) Thatcher, T. L.; Layton, D. W. Deposition, Resuspension, and Penetration of Particles Within a Residence. *Atmos. Environ.* **1995**, 29 (13), 1487–1497.
- (93) Zhao, H.; Stephens, B. Using Portable Particle Sizing Instrumentation to Rapidly Measure the Penetration of Fine and Ultrafine Particles in Unoccupied Residences. *Indoor Air* **2017**, *27* (1), 218–229.
- (94) Liu, Y.; Misztal, P. K.; Xiong, J.; Tian, Y.; Arata, C.; Nazaroff, W. W.; Goldstein, A. H. Detailed Investigation of Ventilation Rates and Airflow Patterns in a Northern California Residence. *Indoor Air* **2018**, 28 (4), 572–584.
- (95) Coleman, B. K.; Lunden, M. M.; Destaillats, H.; Nazaroff, W. W. Secondary Organic Aerosol from Ozone-Initiated Reactions with Terpene-Rich Household Products. *Atmos. Environ.* **2008**, 42 (35), 8234–8245.
- (96) Waring, M. S.; Wells, J. R.; Siegel, J. A. Secondary Organic Aerosol Formation from Ozone Reactions with Single Terpenoids and Terpenoid Mixtures. *Atmos. Environ.* **2011**, *45* (25), 4235–4242.
- (97) Nazaroff, W. W.; Weschler, C. J. Cleaning Products and Air Fresheners: Exposure to Primary and Secondary Air Pollutants. *Atmos. Environ.* **2004**, *38* (18), 2841–2865.
- (98) Singer, B. C.; Destaillats, H.; Hodgson, A. T.; Nazaroff, W. W. Cleaning Products and Air Fresheners: Emissions and Resulting Concentrations of Glycol Ethers and Terpenoids. *Indoor Air* **2006**, *16* (3), 179–191.
- (99) Youssefi, S.; Waring, M. S. Indoor Transient SOA Formation from Ozone+α-Pinene Reactions: Impacts of Air Exchange and Initial Product Concentrations, and Comparison to Limonene Ozonolysis. *Atmos. Environ.* **2015**, *112*, 106–115.
- (100) Hung, D. v.; Tong, S.; Nakano, Y.; Tanaka, F.; Hamanaka, D.; Uchino, T. Measurements of Particle Size Distributions Produced by Humidifiers Operating in High Humidity Storage Environments. *Biosystems Engineering* **2010**, *107* (1), 54–60.
- (101) Rodes, C.; Smith, T.; Crouse, R.; Ramachandran, G. Measurements of the Size Distribution of Aerosols Produced by Ultrasonic Humidification. *Aerosol Sci. Technol.* **1990**, *13* (2), 220–229.

- (102) Sain, A. E.; Dietrich, A. M. Emission of Inhalable Dissolved Drinking Water Constituents by Ultrasonic Humidifiers. *Environ. Eng. Sci.* **2015**, 32 (12), 1027–1035.
- (103) Virudachalam, S.; Long, J. A.; Harhay, M. O.; Polsky, D. E.; Feudtner, C. Prevalence and Patterns of Cooking Dinner at Home in the USA: National Health and Nutrition Examination Survey (NHANES) 2007–2008. *Public Health Nutrition* **2014**, *17* (5), 1022–1030.
- (104) Farmer, N.; Wallen, G. R.; Yang, L.; Middleton, K. R.; Kazmi, N.; Powell-Wiley, T. M. Household Cooking Frequency of Dinner Among Non-Hispanic Black Adults Is Associated with Income and Employment, Perceived Diet Quality and Varied Objective Diet Quality, HEI (Healthy Eating Index): NHANES. *Nutrients* 2019, 11, 2057.
- (105) Thornburg, J. W.; Rodes, C. E.; Lawless, P. A.; Stevens, C. D.; Williams, R. W. A Pilot Study of the Influence of Residential HAC Duty Cycle on Indoor Air Quality. *Atmos. Environ.* **2004**, *38* (11), 1567–1577.
- (106) Bekö, G.; Weschler, C. J.; Wierzbicka, A.; Karottki, D. G.; Toftum, J.; Loft, S.; Clausen, G. Ultrafine Particles: Exposure and Source Apportionment in 56 Danish Homes. *Environ. Sci. Technol.* **2013**, 47 (18), 10240–10248.
- (107) Klein, F.; Farren, N. J.; Bozzetti, C.; Daellenbach, K. R.; Kilic, D.; Kumar, N. K.; Pieber, S. M.; Slowik, J. G.; Tuthill, R. N.; Hamilton, J. F.; Baltensperger, U.; Prévôt, A. S. H.; el Haddad, I. Indoor Terpene Emissions from Cooking with Herbs and Pepper and Their Secondary Organic Aerosol Production Potential. *Sci. Rep.* **2016**, *6*, 36623.
- (108) Klein, F.; Baltensperger, U.; Prévôt, A. S. H.; el Haddad, I. Quantification of the Impact of Cooking Processes on Indoor Concentrations of Volatile Organic Species and Primary and Secondary Organic Aerosols. *Indoor Air* **2019**, 29 (6), 926–942.
- (109) Hussein, T.; Alameer, A.; Jaghbeir, O.; Albeitshaweesh, K.; Malkawi, M.; Boor, B. E.; Koivisto, A. J.; Löndahl, J.; Alrifai, O.; Al-Hunaiti, A. Indoor Particle Concentrations, Size Distributions, and Exposures in Middle Eastern Microenvironments. *Atmosphere* **2020**, *11* (1), 41.
- (110) Li, C.-S.; Lin, W.-H.; Jenq, F.-T. Size Distributions of Submircometer Aerosols From Cooking. *Environ. Int.* **1993**, *19*, 147–154.
- (111) Wallace, L. Indoor Sources of Ultrafine and Accumulation Mode Particles: Size Distributions, Size-Resolved Concentrations, and Source Strengths. *Aerosol Sci. Technol.* **2006**, *40* (5), 348–360.
- (112) Bhangar, S.; Mullen, N. A.; Hering, S. v.; Kreisberg, N. M.; Nazaroff, W. W. Ultrafine Particle Concentrations and Exposures in Seven Residences in Northern California. *Indoor Air* **2011**, *21* (2), 132–144.
- (113) Mullen, N. A.; Liu, C.; Zhang, Y.; Wang, S.; Nazaroff, W. W. Ultrafine Particle Concentrations and Exposures in Four High-Rise Beijing Apartments. *Atmos. Environ.* **2011**, *45* (40), 7574–7582.
- (114) Spilak, M. P.; Frederiksen, M.; Kolarik, B.; Gunnarsen, L. Exposure to Ultrafine Particles in Relation to Indoor Events and Dwelling Characteristics. *Building and Environment* **2014**, *74*, 65–74.
- (115) Miller, S. L.; Facciola, N. A.; Toohey, D.; Zhai, J. Ultrafine and Fine Particulate Matter inside and Outside of Mechanically Ventilated Buildings. *International Journal of Environmental Research and Public Health* **2017**, *14* (2), 128.
- (116) Wheeler, A. J.; Wallace, L. A.; Kearney, J.; van Ryswyk, K.; You, H.; Kulka, R.; Brook, J. R.; Xu, X. Personal, Indoor, and Outdoor Concentrations of Fine and Ultrafine Particles Using Continuous Monitors in Multiple Residences. *Aerosol Sci. Technol.* **2011**, 45 (9), 1078–1089.
- (117) He, C.; Morawska, L.; Hitchins, J.; Gilbert, D. Contribution from Indoor Sources to Particle Number and Mass Concentrations in Residential Houses. *Atmos. Environ.* **2004**, *38* (21), 3405–3415.
- (118) Wallace, L.; Ott, W. Personal Exposure to Ultrafine Particles. *J. Exposure Sci. Environ. Epidemiol.* **2011**, 21 (1), 20–30.
- (119) Less, B.; Mullen, N.; Singer, B.; Walker, I. Indoor Air Quality in 24 California Residences Designed as High-Performance Homes. Science and Technology for the Built Environment 2015, 21 (1), 14–24.

- (120) Koivisto, A. J.; Kling, K. I.; Hänninen, O.; Jayjock, M.; Löndahl, J.; Wierzbicka, A.; Fonseca, A. S.; Uhrbrand, K.; Boor, B. E.; Jiménez, A. S.; Hämeri, K.; Maso, M. D.; Arnold, S. F.; Jensen, K. A.; Viana, M.; Morawska, L.; Hussein, T. Source Specific Exposure and Risk Assessment for Indoor Aerosols. *Sci. Total Environ.* 2019, 668, 13–24. (121) Zhao, J.; Birmili, W.; Hussein, T.; Wehner, B.; Wiedensohler, A. Particle Number Emission Rates of Aerosol Sources in 40 German Households and Their Contributions to Ultrafine and Fine Particle Exposure. *Indoor Air* 2020, DOI: 10.1111/ina.12773.
- (122) Rim, D.; Green, M.; Wallace, L.; Persily, A.; Choi, J.-I. Evolution of Ultrafine Particle Size Distributions Following Indoor Episodic Releases: Relative Importance of Coagulation, Deposition and Ventilation. *Aerosol Sci. Technol.* **2012**, *46* (5), 494–503.
- (123) Persily, A. K. Field Measurement of Ventilation Rates. *Indoor Air* **2016**, 26 (1), 97–111.
- (124) Nazaroff, W. W.; Cass, G. R. Mathematical Modeling of Indoor Aerosol Dynamics. *Environ. Sci. Technol.* **1989**, 23 (2), 157–166.
- (125) Weschler, C. J.; Carslaw, N. Indoor Chemistry. *Environ. Sci. Technol.* **2018**, 52 (5), 2419–2428.